Cyclotron motion in a Penning-trap microwave cavity

Lowell S. Brown, Gerald Gabrielse, and Joseph Tan
Department of Physics, FM-15, University of Washington, Seattle, Washington 98195

K. C. D. Chan
Accelerator Technology Division, Los Alamos National Laboratory, Los Alamos, New Mexico 87545
(Received 15 July 1987)

The cavity shifts in the cyclotron motion of a charged particle in a hyperbolic Penning trap are described using a numerical evaluation of the cavity-mode structure. The frequency shifts are about half as large in the hyperbolic cavity as in a cylindrical cavity of equivalent size. However, this still implies an error in the $g-2$ experiment that is easily five times the present statistical uncertainty. To account for slit electrodes and imperfect tolerances in existing traps, experimental measurements of the mode structure are still needed. The resonant frequencies of a microwave cavity can be measured very precisely. We show here that an accuracy of 10% in the measurements of certain coupling constants is sufficient to compute the shifts for the $g-2$ experiment at the level of one part in 10^9.

I. INTRODUCTION

A long series of experiments at the University of Washington has succeeded in isolating a single electron and measuring its magnetic moment, or rather, g factor with unprecedented precision.[1,2] The most recent experiment[3] has a statistical accuracy of five parts in 10^{10}. There is, however, a systematic effect that may well be an order of magnitude larger. This is the correction brought about by the radiative electromagnetic interaction of the single electron with the metallic walls of the Penning trap that surrounds it. The trap forms a microwave cavity whose modes interact with the cyclotron motion. This interaction significantly modifies the observed cyclotron damping rate[4] and also shifts the cyclotron frequency ω_c to

$$\bar{\omega}_c=\omega_c+\Delta\omega_c \ . \tag{1.1}$$

The physics of this shift has already been extensively discussed[2,5–7] and so we shall provide here only the briefest review. The cavity shift can easily be as large[6] as $\Delta\omega_c/\omega_c\approx 5\times 10^{-12}$. To see that this is a significant correction to the $g-2$ experiment, we note that the measured anomaly is (essentially) determined by

$$a=\frac{g-2}{2}=\frac{\omega_s-\omega_c}{\omega_c} \ , \tag{1.2}$$

where ω_s is the spin precession frequency. Thus, if the cavity shift (1.1) is not accounted for, it gives rise to a systematic error,

$$\frac{\Delta a}{a}=\frac{1}{a}\frac{\Delta\omega_c}{\omega_c} \ . \tag{1.3}$$

Since $a\approx 1\times 10^{-3}$, one sees that the cavity shift may give $\Delta a/a\approx 5\times 10^{-9}$, which is indeed an order of magnitude larger than the statistical accuracy of the experiment.

The purpose of the present paper is to provide a detailed account of the cavity shift for the geometry of the actual experiment, a cavity formed by hyperbolic surfaces of revolution. This we shall do in part by means of a numerical evaluation of the mode structure for such cavities. In actual experimental traps, small impressions in the dimensions can significantly shift the cavity eigenfrequencies, limiting the direct applicability of these numerical calculations. Therefore, experimental measurements of the mode structures will be required to get a sufficient account of the cavity shifts. We shall describe the accuracy needed in such measurements.

Before describing the results, we sketch the basic theory. The Penning trap consists of a strong uniform magnetic field along the z axis superimposed over a weak electrostatic potential $V(\mathbf{r})$, giving the equation of motion

$$\dot{\mathbf{v}}-\boldsymbol{\omega}_c\times\mathbf{v}+\frac{e}{m}\nabla V(\mathbf{r})+\tfrac{1}{2}\gamma_c\mathbf{v}=0 \ . \tag{1.4}$$

Here $\boldsymbol{\omega}_c=\omega_c\hat{\mathbf{z}}$ is the cyclotron frequency of the particle's rotation in the magnetic field alone, and

$$\gamma_c(\omega_c)=4e^2\omega_c^2/3mc^3 \tag{1.5}$$

is the free-space damping constant of this motion. Radiative effects for the other submotions implied by the equation of motion (1.4) are negligible since they are much slower. Our interest is in the modification of the cyclotron motion when it takes place about the center of an axially symmetric conducting cavity, with the orbit size very small in comparison to the size of the cavity. Neglecting insignificant image magnetic forces, the presence of the surrounding metallic cavity alters the equation of motion to read

$$\dot{\mathbf{v}}-\boldsymbol{\omega}_c\times\mathbf{v}+\frac{e}{m}\nabla V(\mathbf{r})+\tfrac{1}{2}\gamma_c\mathbf{v}=\frac{e}{m}\mathbf{E}'(\mathbf{r}) \ . \tag{1.6}$$

Here $\mathbf{E}'(\mathbf{r})$ is the electric field at the position $\mathbf{r}(t)$ of the charged particle brought about by the presence of the cavity. It is the electric field acting on the particle omitting the trap field $[-\nabla V(\mathbf{r})]$ and also excluding the self-field of the particle. This proper field is accounted for by the use of the observed (renormalized) mass m and the radiative dissipation described by the damping constant γ_c. It is convenient to split the field $\mathbf{E}'$ into longitudinal and transverse parts. The longitudinal part gives the Coulomb interaction of the charged particle with the effective image charges that represent the cavity walls. This part provides merely a small alteration in the trapping potential $V(\mathbf{r})$ which is experimentally unobservable. The transverse field gives the radiative interaction of the charged particle with the cavity. It may be expressed as

$$E_k^{(T)'}(t,\mathbf{r})=-\frac{\partial}{\partial t}\int dt' \sum_{l=1}^{3} D'_{kl}(t-t';\mathbf{r},\mathbf{r}'(t'))e\mathbf{v}_l(t')/c^2 , \tag{1.7}$$

where $D'_{kl}(t-t';\mathbf{r},\mathbf{r}')$ is the alteration of the retarded Green's function due to the cavity. Since the charged particle is confined to a small region near the center of the cavity, it suffices to set $\mathbf{r}=\mathbf{r}(t)=\mathbf{0}$ and $\mathbf{r}(t')=\mathbf{0}$. Inserting the field solution (1.7) into the equation of motion (1.6) and Fourier transforming to exhibit the steady-state solution yields

$$\omega-\omega'_c+i\gamma_c/2=-\omega r_0 \tilde{D}'_{xx}(\omega;0,0) , \tag{1.8}$$

where $r_0=e^2/mc^2\simeq 2.8\times 10^{-13}$ cm is the classical electron radius. The effect of the trapping potential is to replace the cyclotron frequency ω_c by the slightly modified frequency ω'_c, but this is irrelevant for our calculation of the cavity shift.

The full Green's function $\tilde{D}_{kl}(\omega;\mathbf{r},\mathbf{r}')$ which includes the free-space contribution as well as the cavity correction is defined by

$$\left[-\nabla^2-\frac{\omega^2}{c^2}\right]\tilde{D}_{kl}(\omega;\mathbf{r},\mathbf{r}')=4\pi\left[1-\nabla\frac{1}{\nabla^2}\nabla\right]_{kl}\delta(\mathbf{r}-\mathbf{r}') . \tag{1.9}$$

It may be expressed as a sum over the complete set of cavity modes,

$$\tilde{D}_{kl}(\omega;\mathbf{r},\mathbf{r}')=c^2\sum_{N=1}^{\infty}\frac{\mathcal{E}_{N,k}(\mathbf{r})\mathcal{E}_{N,l}(\mathbf{r}')}{\omega_N^2-\omega^2} . \tag{1.10}$$

Here ω_N is the angular eigenfrequency of the Nth mode, and $\mathcal{E}_{N,k}(\mathbf{r})$ is the kth vector component of the electric field mode function whose tangential components vanish on the cavity surface. Substituting this construction into the Green's-function equation, multiplying by $\mathcal{E}_{M,l}(\mathbf{r}')$, summing over l, and integrating $\mathbf{r}'$ over the volume of the cavity, we learn that the normalization of the vector mode functions is given by

$$\frac{1}{4\pi}\sum_{l=1}^{3}\int(d\mathbf{r}')\mathcal{E}_{N,l}(\mathbf{r}')\mathcal{E}_{M,l}(\mathbf{r}')=\delta_{N,M} . \tag{1.11}$$

The Green's function $\tilde{D}'_{xx}(\omega;0,0)$ which appears in the frequency shift (1.8) has the same poles and residues as those given by the sum in Eq. (1.10), but the free-space function is removed from $\tilde{D}_{xx}(\omega;0,0)$ to form $\tilde{D}'_{xx}(\omega;0,0)$. Thus, except for an (infinite) constant that is absorbed into the mass normalization, the two functions can differ only by an entire function—a polynomial in ω^2. Let us denote by L a typical length of the cavity. The dimension of $\tilde{D}'_{xx}(\omega;0,0)$ is L^{-1}. Hence this polynomial must contain an overall factor of L^{-1} times powers of the dimensionless variable (ω^2L^2/c^2). But this polynomial must vanish as the cavity becomes very large; it must vanish in the limit $L\to\infty$. Hence it can contain only a constant term κ/L, where κ is a dimensionless number which depends on the shape of the cavity. Therefore

$$\tilde{D}'_{xx}(\omega;0,0)=\frac{\kappa}{L}+\sum_{N=1}^{\infty}\frac{c^2\mathcal{E}_{N,x}(0)^2}{\omega_N^2}\frac{\omega^2}{\omega_N^2-\omega^2} . \tag{1.12}$$

As a check on this formula, one may verify from the explicit expressions given in Ref. 6 that the modified (subtracted) sum in Eq. (1.12) converges for the case of a cylindrical cavity. Inserting Eq. (1.12) into the frequency shift (1.8), we obtain

$$\omega-\omega'_c=-\omega\frac{r_0}{L}\left[\kappa+\omega^2\sum_{N=1}^{\infty}\frac{\lambda_N^2}{\omega_N^2-\omega^2-i\omega\Gamma_N}\right] . \tag{1.13}$$

Here we have included the decay constants Γ_N for the cavity modes with $Q_N=\omega_N/\Gamma_N$ the corresponding quality factor of a mode; but at the same time, we must delete the term $i\gamma_c/2$ which appears on the left-hand side in Eq. (1.8) in order that the absorptive part of the sum on the right-hand side reproduce the free-space decay constant $-\gamma_c/2$ in the limit of an infinitely large cavity made of lossy material.[6] The sign in the damping term $-\omega\Gamma_N$ is dictated by the causal requirement of decay, rather than growth, of the cyclotron orbit with time. This simple modification of the denominator suffices to describe cavity dissipation since, generally, $Q_N\gg 1$. The mode coupling constants λ_N^2 are given by[8]

$$\lambda_N^2=L\left[\frac{c\mathcal{E}_{N,x}(0)}{\omega_N}\right]^2 , \tag{1.14}$$

and they are dimensionless.

The "subtraction constant" κ appearing in Eq. (1.13) accounts for the finite renormalization of the electron mass brought about by the presence of the cavity, for it corresponds to a term multiplying the acceleration $\dot{\mathbf{v}}$ in the equation of motion. Once this subtraction has been made, the sum in Eq. (1.13) converges. This constant can be calculated for a right-cylindrical cavity of radius R and length $2L$ using the analytic expressions given in Ref. 6. The result for a range of aspect ratios R/L is shown in Fig. 1. In the parallel-plate limit $R/L\to\infty$, one has $\kappa=-\frac{1}{2}\ln 2=-0.347$. We see that κ is rather insensitive to the aspect ratio R/L. As will be shown in Sec. II, κ also makes quite a small contribution to the cavity shift $\omega-\omega'_c$ in the frequency range of experimental interest. Hence, although we cannot compute κ for the hyperbolic

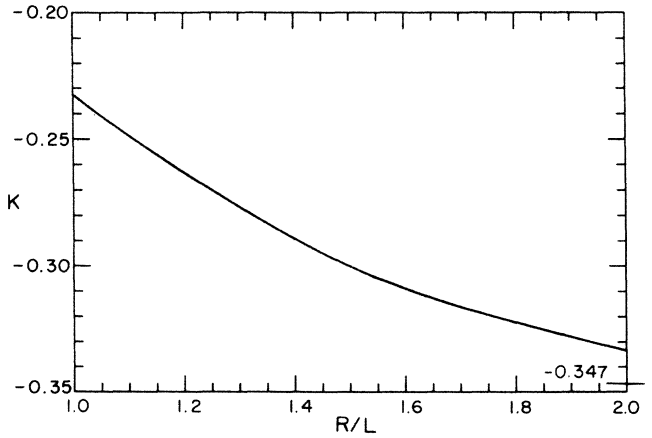

FIG. 1. Subtraction constant κ as a function of R/L for a cylindrical cavity of radius R and length $2L$. The tickmark marks the $R \to \infty$ limiting value. [The evaluation is made from Eqs. (3.21) and (4.28) of Ref. 6].

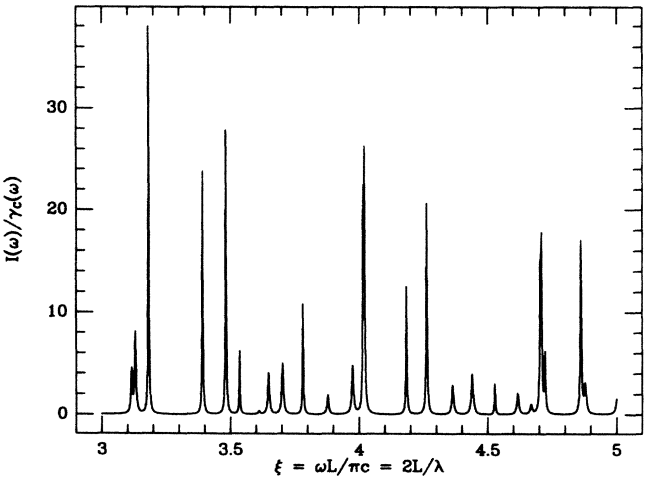

FIG. 2. Decay constant $I(\omega)/\gamma_c(\omega)$ for a charged particle moving in a small orbit about the axis and centered in the midplane of a cylindrical cavity with $Q=1000$ and an aspect ratio $R/L=1.186$. The solid line is the analytic result of Ref. 6. The pole sum given by Eq. (1.13) using the exact analytic results of Ref. 6 for ω_N and λ_N with only a finite number of poles taken in the bandwidth $-0.5<\xi_N-\xi<0.5$ is also plotted as a dotted line, but the fit is so good that this dotted line is not visible.

cavity of interest to the accuracy that we need, it is sufficient to use the κ value for a cylindrical cavity of the same aspect ratio.

In Sec. II we describe the accuracy achieved in the frequency shift for a cylindrical cavity when one sums over only a finite number of modes, and how well the sum with numerically evaluated mode frequencies ω_N and couplings λ_N agrees with the exact analytic result. With these tests in hand, we then go on in Sec. III to describe our results for the hyperbolic cavity. Since these results depend very sensitively on the precise geometry of the cavity, we discuss in Sec. IV the feasibility of using measured values of the cavity-mode frequencies ω_N and coupling constants λ_N^2 for the actual experimental trap. Section V summarizes our results.

II. POLE FITS

In this section we illustrate the accuracy of our work by computing the cavity shifts for a cylindrical shape with aspect ratio $R/L=1.186$. This is the geometry selected for a cylindrical trap whose properties are now being studied.[9] First we shall show how well a finite sum of pole terms reproduces the exact analytic result when the exact analytic forms for the frequencies and couplings are used. Then we shall compare the exact analytic result with a finite sum formed with the numerically evaluated frequencies and couplings.

A. Finite sum

In Figs. 2 and 3 we plot the decay constants and frequency shifts for a cylindrical cavity (with $R/L=1.186$) as a function of the scaled, dimensionless frequency variable

$$\xi=\frac{\omega L}{\pi c}=\frac{2L}{\lambda}\ , \tag{2.1}$$

which is the number of wavelengths that fit between the two flat end plates. The range shown, $3<\xi<5$, corresponds to that of primary interest in the $g-2$ experiments. For a cylindrical cavity, the widths of the TM modes, $\Gamma_N^{(M)}=\Gamma^{(M)}$, are all the same, while those of the TE modes, $\Gamma_N^{(E)}$, are about half as large[6] as $\Gamma^{(M)}$. Thus the cavity dissipation is accounted for by setting $\Gamma^{(M)}\simeq\omega/Q^{(M)}$ and $\Gamma^{(E)}\sim\omega/Q^{(E)}$, with $Q^{(E)}=2Q^{(M)}=Q$. The plots are drawn for $Q=1000$. The decay constant $I(\omega)$ is the negative of twice the imaginary part of the complex frequency shift $\omega-\omega_c'$. It appears in Fig. 2, scaled by the free-space cyclotron damping constant

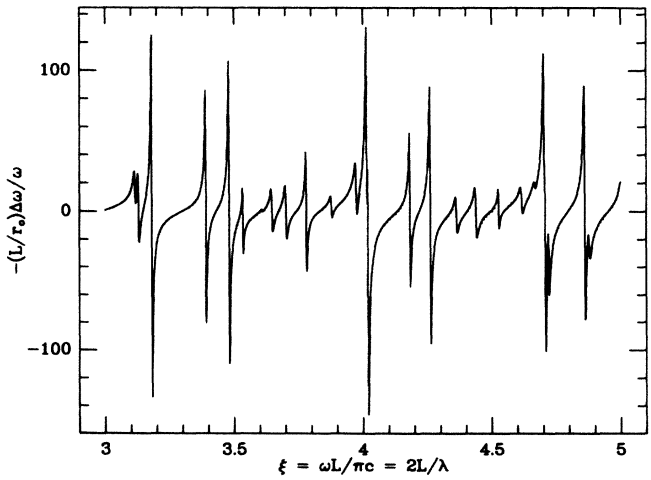

FIG. 3. Scaled frequency shift $-(L/r_0)\Delta\omega/\omega$ for the cylindrical cavity of Fig. 2 with the solid and dotted lines having the same significance as in Fig. 2.

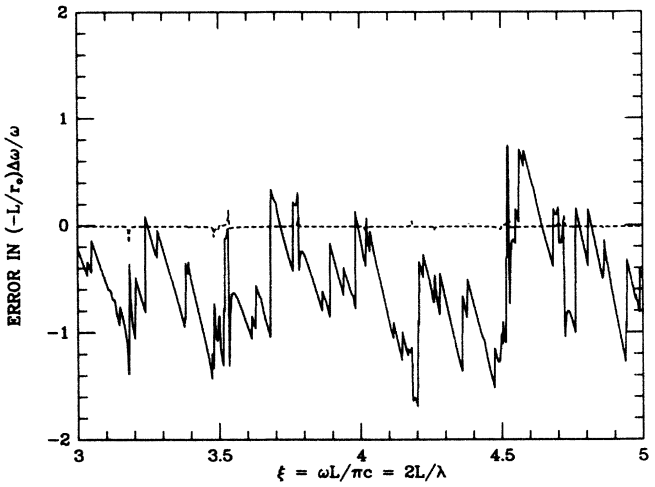

FIG. 4. Differences in the analytic result and the finite sum of poles shown in Figs. 2 and 3. The solid curve gives the errors in the scaled frequency shifts $-(L/r_0)\Delta\omega/\omega$; the dashed curve, the errors in the scaled decay constants $I(\omega)/\gamma_c(\omega)$.

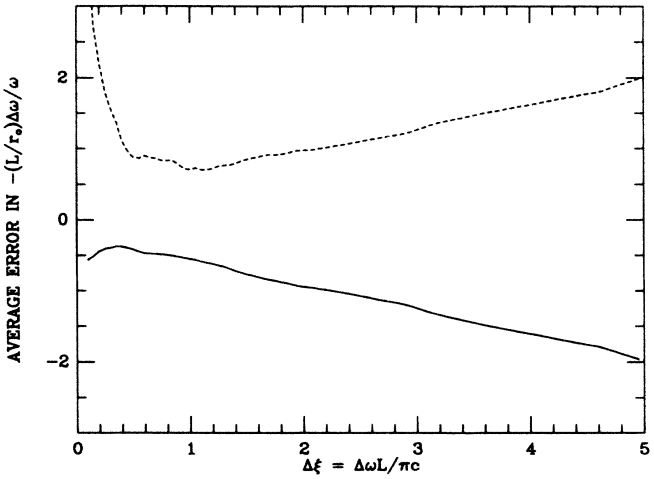

FIG. 5. Averaged error in the pole sum for the scaled frequency shift $-(L/r_0)\Delta\omega/\omega$, averaged over the frequency interval $3<\xi<5$. The solid curve displays this error as a function of the bandwidth $\Delta\xi$; the dashed curve, the corresponding rms error. The bandwidth $\Delta\xi$ limits the scaled eigenfrequencies ξ_N that are used in the pole sum to the interval $-0.5\Delta\xi<\xi_N-\xi<0.5\Delta\xi$, thereby retaining only a finite number of terms.

$\gamma_c(\omega)$. The frequency shift $\Delta\omega$ is the real part of $\omega-\omega_c'$. The fractional frequency shift $\Delta\omega/\omega$ scaled by r_0/L appears in Fig. 3. For a typical $g-2$ trap, $r_0/L \approx 5\times10^{-13}$, and one division of the ordinate (20 scale units) corresponds to a fractional shift $\Delta\omega/\omega$ of approximately 10×10^{-12}, which is 20 times the present statistical error in the experiments.[3]

The solid lines in Figs. 2 and 3 are the exact analytic results of Ref. 6. Superimposed on these graphs are dotted lines that give the result for a finite truncation of the pole sum given in Eq. (1.13) with $\kappa=-0.27$ and the eigenfrequencies ω_N and couplings λ_N evaluated from the analytic forms given in Ref. 6. The dotted curves are so close to the exact analytic results (solid lines) as to be invisible for the most part. It should be noted that the subtraction constant κ makes quite a small contribution ($\Delta\omega/\omega\approx1\times10^{-13}$). The truncated sum was evaluated only for poles with eigenfrequencies ω_N that lie in a fixed "bandwidth" about the frequency ω. It is convenient to characterize this bandwidth in terms of the dimensionless frequency variable ξ and denote the bandwidth by $\Delta\xi$. A bandwidth $\Delta\xi=1.0$ was used in Figs. 2 and 3 so that, a given frequency ξ, at the mode sum includes those resonant-cavity frequencies ξ_N that lie in the interval $-0.5<\xi_N-\xi<0.5$. This bandwidth corresponds to the inclusion of approximately 15 modes in the sum.

To exhibit the very small discrepancies between the truncated pole sum and the exact results, their differences are plotted in Fig. 4. The solid curve represents the differences in the frequency shift, the dashed curve the decay-constant differences, with both scaled as in Figs. 2

TABLE I. Cylindrical cavity-mode structure for $R/L=1.186$.

	ξ eigenvalues $=\xi_N$			Coupling constants λ_N^2	
No.	Exact	Numerical	Type	Exact	Numerical
1	0.703	0.705	*E*01	1.221	1.323
2	1.143	1.142	*M*01	0.130	0.138
3	1.516	1.517	*E*02	0.556	0.629
4	1.579	1.585	*E*11	0.242	0.257
5	1.819	1.822	*M*11	0.183	0.195
6	1.948	1.943	*M*02	0.028	0.030
7	2.073	2.077	*E*12	0.290	0.343
8	2.345	2.344	*E*03	0.356	0.393
9	2.407	2.406	*M*12	0.107	0.109
10	2.548	2.556	*E*21	0.093	0.102
11	2.703	2.709	*M*21	0.104	0.118
12	2.738	2.739	*E*13	0.261	0.302
13	2.776	2.766	*M*03	0.010	0.012
14	2.881	2.886	*E*22	0.150	0.175
15	3.115	3.117	*M*13	0.055	0.007

and 3. Clearly, the decay constants are fit very well indeed. The jitter in the frequency-shift error, for the most part, probably arises from computer-round-off error in evaluating the exact "analytical" result, which entails computing a sum of Bessel functions, which is done only with limited accuracy. At any rate, we see that the error in $(\Delta\omega/\omega)(L/r_0)$ is at worst approximately 1.0, corresponding to an error in $\Delta\omega/\omega$ of approximately 5×10^{-13} for a typical trap dimension.

The bandwidth $\Delta\xi$ that is needed for an accurate representation by the pole sum can be accessed by calculating the average of the frequency differences shown in Fig. 4, or the rms averaging of these differences, averaged over the interval of interest $3<\xi<5$, as a function of $\Delta\xi$, not only for $\Delta\xi=1$ as shown in Fig. 4. The result of this procedure is shown in Fig. 5. The solid line gives the average difference, the dashed line the rms average difference, as a function of the bandwidth $\Delta\xi$. All modes below ξ tend to have larger effective-field strengths than the modes above ξ. The average error thus increases with $\Delta\xi$, until the bandwidth exceeds the threshold 2ξ, when all modes below ξ are exhausted. A further increase in bandwidth decreases the average error, with error vanishing as $\Delta\xi\rightarrow\infty$, the limit of the convergent pole sum, Eq. (1.13).

B. Numerical results

We have just seen that a judiciously chosen finite pole sum provides an accurate description of the shifts for a cylindrical cavity. Thus such a sum should also give an accurate description of the shifts within a hyperbolic cavity, provided that the eigenfrequencies ω_N and coupling parameters λ_N can be evaluated sufficiently well by using numerical techniques—the only theoretical method available for the hyperbolic cavity. The computer calculation that we shall use is the Los Alamos National Laboratory—Deutsches Elektronen-Synchotron (LANL—DESY) program URMEL-T.[10] To test its accuracy, it was first used to compute the eigenfrequencies and coupling parameters for the cyclindrical cavity with aspect ratio $R/L=1.186$. The results are

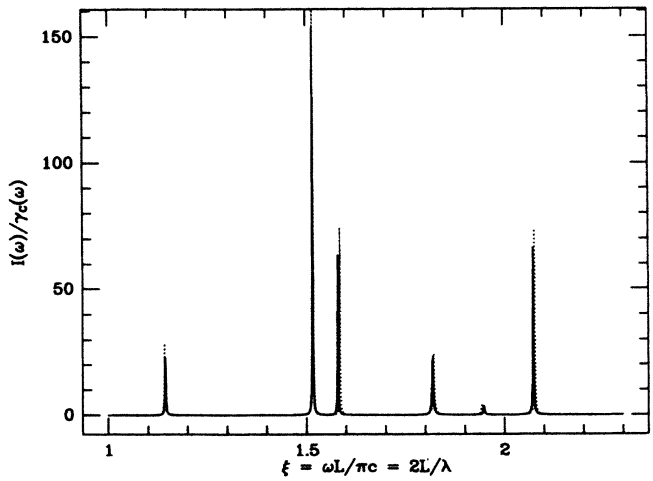

FIG. 6. Same as Fig. 2 but with the numerically evaluated ω_N and λ_N.

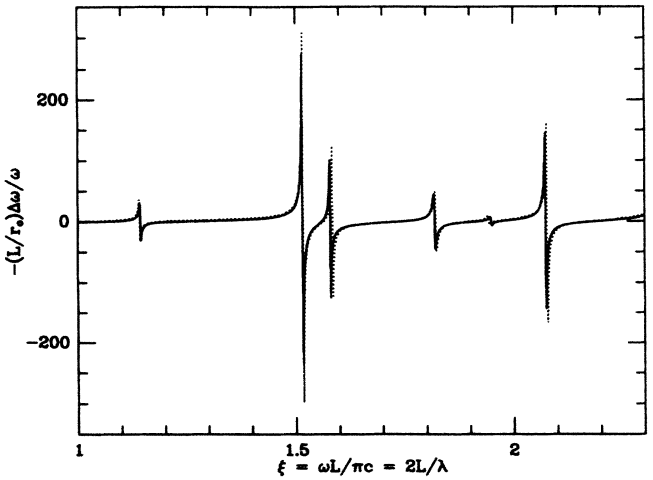

FIG. 7. Same as Fig. 3 but with the numerically evaluated ω_N and λ_N.

given in Table I along with the exact, analytic results of Ref. 6. We see that the errors in the calculated values of the eigenfrequencies are on the average approximately 0.2% and, in any case, do not exceed 0.4%. The errors in the numerical evaluation of the coupling constants are, on the other hand, about two orders of magnitude larger. The last entry in the table has an 87% error because the parameters of the numerical method were not optimized.

Figures 6 and 7 show the decay constants and frequency shifts just as in Figs. 2 and 3, but now using the numerical evaluation of the eigenfrequencies and coupling parameters that are given in Table I. We see that the positions of the resonant frequencies for the calculated result (dotted line) are only slightly displaced from the exact locations shown by the solid line. Although the error very near the resonant frequencies tends to be proportional to the error in the coupling constant, the frequencies of the zero-shift points between modes are only slightly affected. We shall examine this point in detail in Sec. IV.

III. HYPERBOLIC CAVITY

Having illustrated the accuracy of the pole sum used with the analytic mode structure and couplings for the cylindrical cavity, and of the corresponding numerical results using Table I, we shall now employ the pole sum to obtain the cavity shifts and decay constants in a hyperbolic trap with the help of the calculated numerical values in Table II. But before going further, it is important to consider the limitations on this numerical model, since geometrical deviations of an experimental trap from the idealized geometry of the model may not be negligible.

To make an estimate of such deviations, we take the analytic calculations for the cylindrical cavity and ask how much change in the mode structure is incurred by a change of 1% in the aspect ratio R/L. Figure 8 compares the decay constant as a function of the dimensionless frequency [Eq. (2.1)] for the aspect ratios 1.186 (solid line) and 1.200 (dotted line). The corresponding scaled

frequency shift is given in Fig. 9. Not surprisingly, some of the mode frequencies shift in proportion to the dimension change. The absorptive curves in Fig. 8 show that such shifts in the positions of the poles can be as large as the separation between two adjacent modes. Figure 9 shows that the frequencies of the zero-shift point can be moved to regions of maximal frequency shifts. Hence uncertainty in the experimental-trap geometry on the level of a few percent precludes a close comparison of a model with experiment. A pole-sum computation of the cavity effects for the actual hyperbolic trap is of qualitative significance only. This is the reason that we were

TABLE II. Hyperbolic cavity-mode structure for $\rho_0/z_0=\sqrt{2}$.

No.	ξ eigenvalues $=\xi_N$	Coupling constants λ_N^2
1	0.443	0.300
2	0.663	0.707
3	0.926	0.118
4	1.185	0.466
5	1.292	0.049
6	1.338	0.043
7	1.469	0.065
8	1.566	0.272
9	1.694	0.042
10	1.729	0.040
11	1.740	0.317
12	1.899	0.071
13	1.972	0.003
14	2.022	0.034
15	2.079	0.344
16	2.147	0.011
17	2.237	0.018
18	2.300	0.119
19	2.353	0.079
20	2.406	0.082
21	2.471	0.048
22	2.535	0.003
23	2.563	0.066
24	2.670	0.005
25	2.694	0.283
26	2.731	0.138
27	2.739	0.006
28	2.837	0.110
29	2.895	0.003
30	2.954	0.080
31	2.988	0.108
32	3.076	0.043
33	3.106	0.015
34	3.137	0.057
35	3.162	0.002
36	3.178	0.053
37	3.285	0.000
38	3.309	0.181
39	3.324	0.126
40	3.375	0.018
41	3.446	0.073
42	3.459	0.001
43	3.515	0.106
44	3.571	0.200
45	3.711	0.025

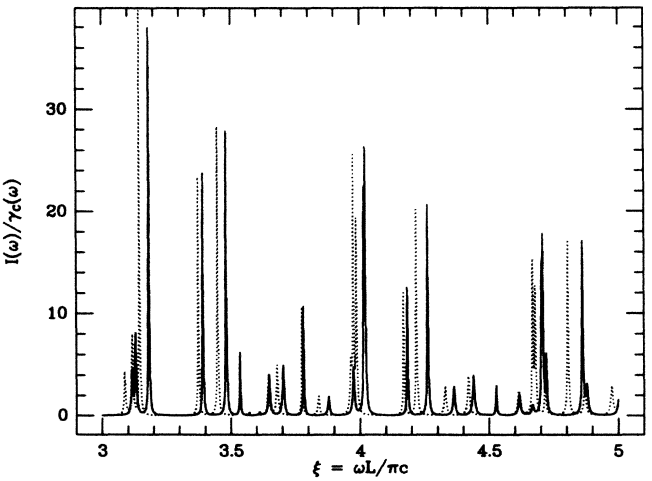

FIG. 8. Comparison of decay constant $I(\omega)/\gamma_c(\omega)$ between two cylindrical cavities of slightly different aspect ratios, but having the same $Q=1000$. The solid line is for $R/L=1.186$; the dashed line, $R/L=1.20$. Both curves are computed using the exact analytic results in Ref. 6.

satisfied with the accuracy of the numerical work for the cylindrical cavity given above, which also indicates the numerical accuracy of the results for a hyperbolic trap that we now present. For the same reaon, we can ignore the small contribution of the subtraction constant κ.

The calculated numerical values for the mode frequencies and couplings in Table II are computed for a hyperbolic trap truncated as shown in Fig. 10. The end-cap electrodes and ring electrode are hyperbola of revolution generated, respectively, by

$$z^2=z_0^2+\rho^2/2 \tag{3.1a}$$

and

$$z^2=\tfrac{1}{2}(\rho^2-\rho_0^2)\ . \tag{3.1b}$$

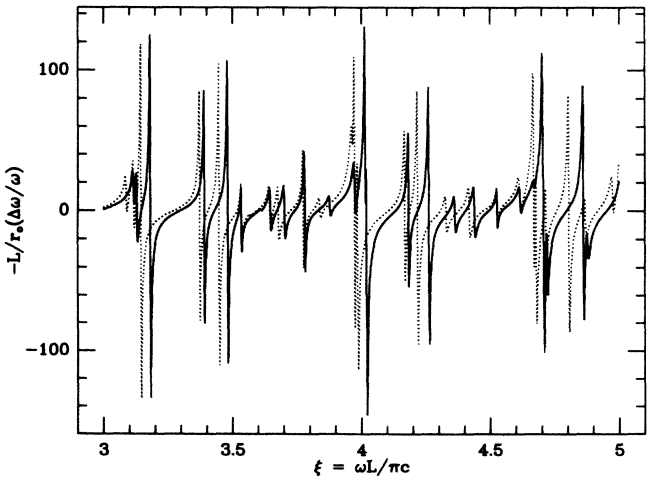

FIG. 9. Comparison of the scaled frequency shift $-(L/r_0)(\Delta\omega/\omega)$ for the cylindrical cavities in Fig. 8 with the same line significance.

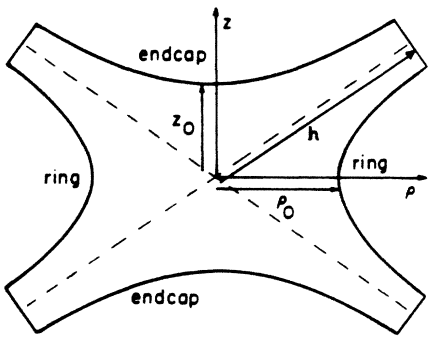

FIG. 10. Schematic diagram of the hyperbolic cavity used in the computation of Table II. The electrodes are hyperbola of revolution about the z axis, with the end caps and ring described, respectively, by $z^2=z_0^2+\rho^2/2$ and $z^2=\frac{1}{2}(\rho^2-\rho_0^2)$. The aspect ratio $\rho_0/z_0=1.414$. The truncation regions are closed with flat rings whose perpendicular distance to the origin is $h/z_0=2.800$, centered about the asymptotes (dashed lines).

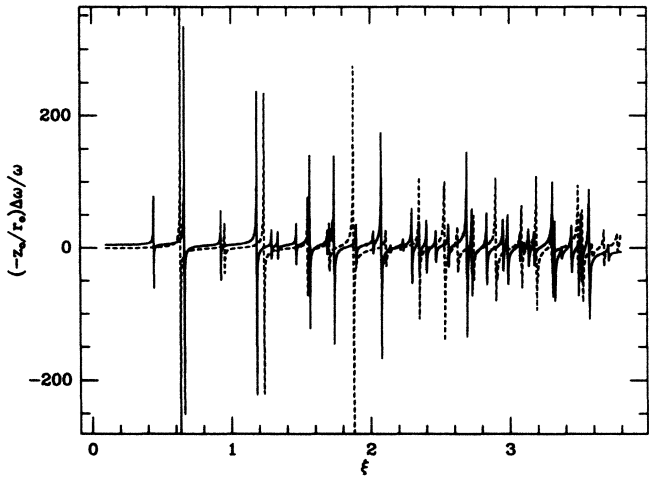

FIG. 12. Scaled frequency shifts $-(z_0/r_0)(\Delta\omega/\omega)$ for the hyperbolic cavity in Fig. 10 (solid line). The dashed line is for a cylindrical cavity with $R/L=1.5$. For the cylinder, z_0 is set to the half length L.

The aspect ratio is given by $\rho_0/z_0=\sqrt{2}$. Flat compensation ring electrodes terminate the truncation region, centered about the asymptote with the perpendicular distance from the origin given by $h/z_0=2.80$. Using Table II with Eq. (1.13), we obtain the decay constant as a function of the dimensionless frequency variable

$$\xi=\frac{\omega z_0}{\pi c}\ , \tag{3.2}$$

as show in Fig. 11. The scaled frequency shift $-(z_0/r_0)(\Delta\omega/\omega)$ is a function of ξ, as shown in Fig. 12. The dashed curves are for a cylindrical cavity with aspect ratio $R_0/z_0=1.5$ and the same $Q=1000$. We see in Fig. 12 that the shifts in the cylindrical cavity are about twice as large as those in the hyperbolic cavity, for the most part. This is to be expected, since the modes are about half as dense in the cylindrical trap as in the hyperbolic trap, owing to the higher degree of symmetry in the cylinder.

IV. POSSIBLE EXPERIMENTAL LOCATION OF MINIMUM CYCLOTRON FREQUENCY SHIFTS

The microwave modes in a hyperbolic Penning trap have been observed[11] by a bolometric technique that monitors the temperature of the axial center-of-mass motion of a cloud of electrons. This method has demonstrated that the eigenfrequencies of a microwave cavity can be determined to a precision of better than one part in 10^4. On the other hand, the coupling constants are

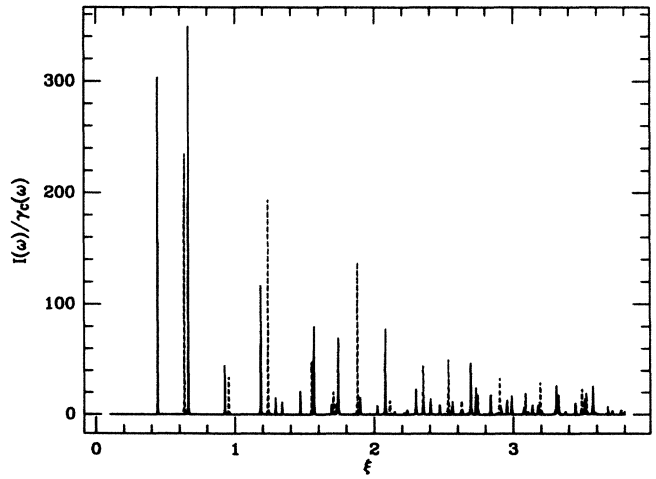

FIG. 11. Decay constant $I(\omega)/\gamma_c(\omega)$ for the hyperbolic cavity shown in Fig. 10 (solid line). The dashed line is for a cylindrical cavity of comparable aspect ratio 1.5 and the same $Q=1000$. For the cylindrical cavity, z_0 is set to the half length L.

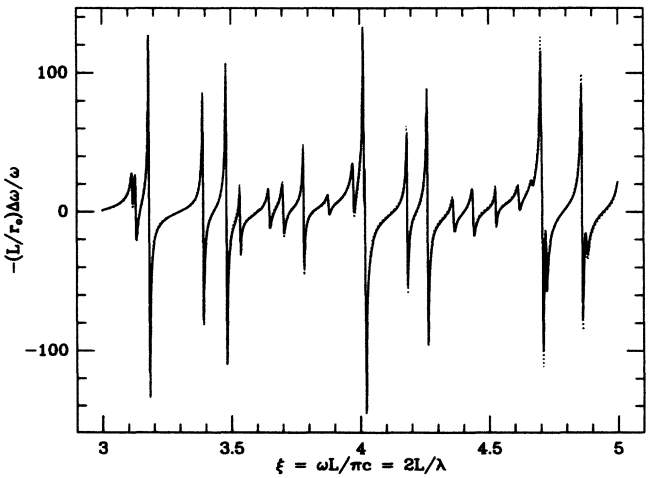

FIG. 13. Scaled frequency shifts $-(L/r_0)\Delta\omega/\omega$ for the cylindrical cavity using the pole-sum equation (1.13). The solid line uses the exact analytic results of Ref. 6 for ω_N and λ_N. The dashed line corresponds to random perturbations in λ_N by 10%.

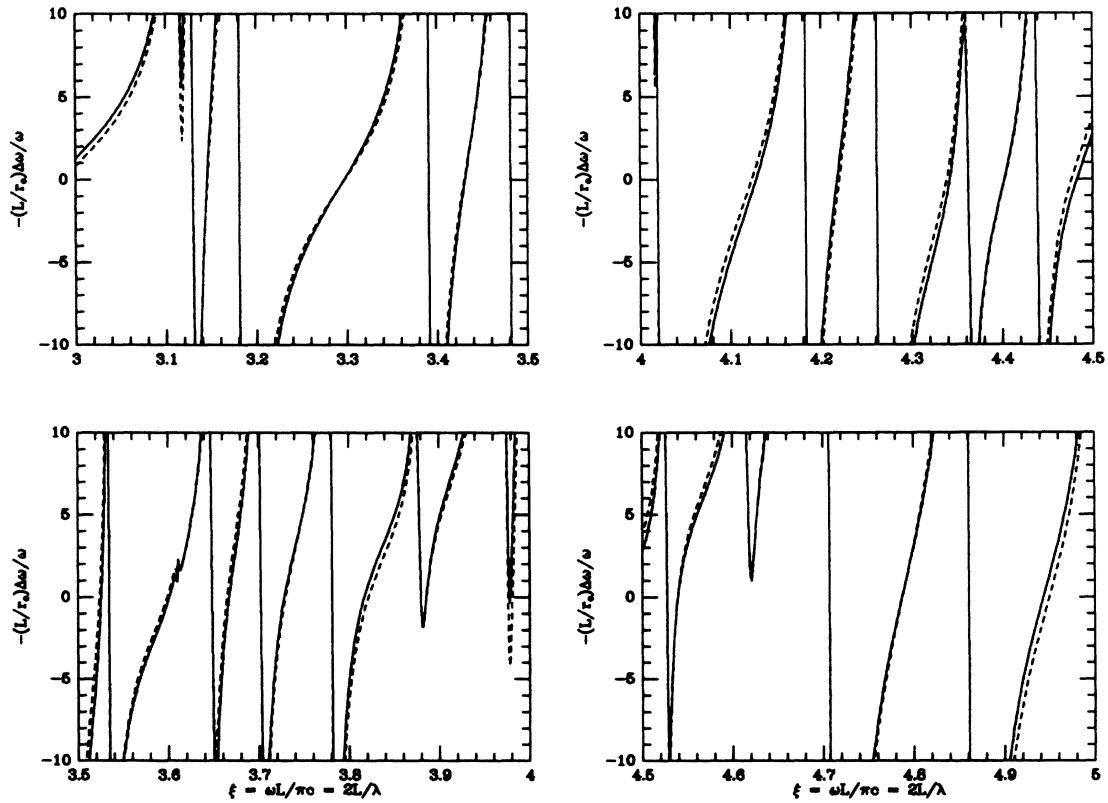

FIG. 14. Magnification of Fig. 13 at the regions of experimental interest.

difficult to measure to better than 10%. This technique so far measures only the relative coupling strengths of the cavity modes. To use this result in a truncated pole sum, the absolute coupling strength of one mode must also be determined. In this section, we shall investigate how well the cyclotron frequencies can be located which give minimal frequency shifts, when the coupling strengths are known only inaccurately.

As a simple estimate, consider the error in the contribution from the nearest mode to the cavity shift if the coupling constant λ_N^2 of this mode has some error $\delta\lambda_N^2$. The ratio of the corresponding error in the frequency shift, $\delta\Delta\omega$, to the maximum shift caused by the mode, $\Delta\omega_{\max}$, has a simple form many linewidths away from the mode frequency ω_N,

$$\frac{\delta\Delta\omega}{\Delta\omega_{\max}}=\frac{\delta\lambda_N^2}{\lambda_N^2}\frac{\Gamma_N}{\omega-\omega_N}=\frac{\delta\lambda_N^2}{\lambda_N^2}\frac{1}{Q}\frac{\omega_N}{\omega-\omega_N}\ . \tag{4.1}$$

From Fig. 3 we see that the average mode separation in the dimensionless frequency ξ is approximately 0.1 for the range of experimental interest where $\xi\simeq 4.0$. Taking $\omega-\omega_N$ to be half of this average mode separation gives

$$\frac{\omega_N}{\omega-\omega_N}=\frac{\xi_N}{\xi-\xi_N}\simeq\frac{4.0}{0.05}\simeq 80\ . \tag{4.2}$$

Accordingly, for a 10% error in the coupling strength, $\delta\lambda_N^2/\lambda_N^2=0.1$, and for the typical quality factor $Q=1000$, we have

$$\frac{\delta\Delta\omega}{\Delta\omega_{\max}}\simeq 0.01\ . \tag{4.3}$$

Since for $Q=1000$, $\Delta\omega_{\max}/\omega_c$ is no larger than approximately 100 parts in 10^{12}, the error near the zero-shift frequencies is less than about one part in 10^{12}.

To give a more accurate estimate, we plot in Fig. 13 the frequency shifts for an aspect ratio of 1.186 and $Q=1000$ with the coupling constants of the cylindrical modes randomly increased or reduced by 10%; the solid line is the unperturbed result. Figure 14 is a magnification of Fig. 13. We note that the deviations are well within our simple estimate for a remarkably wide range of values, including the zero-shift frequencies. Thus an experimental precision of 10% in the measurement of the coupling constants is sufficient for locating the null-shift frequencies at a one part in 10^{12} level.

V. SUMMARY AND CONCLUSION

We have tested the truncated pole sum, Eq. (1.13), using an appropriate number of modes with the exact analytic forms of the eigenfrequencies and coupling constants for a cylindrical cavity. This gives sufficiently precise results. Extending this to the hyperbolic Penning trap with the help of the numerically-determined cavity-mode structure, we find that the cavity shifts in the hyperbolic trap are approximately half as large as those in a cylindrical trap of equivalent size. But this still implies an error in the $g-2$ experiment that is easily five times

the present statistical uncertainty.

The precision in the actual-trap geometry is unfortunately not sufficient to permit using the numerical evaluations to model the actual experimental trap and locate the frequencies that give minimum cavity shifts. Experimental measurements of the mode structure, therefore, must be employed to determine these minimum-shift frequencies. A simple calorimetric technique[10] can measure very precisely the resonant frequencies of a microwave cavity. We have shown here that a 10% accuracy in the measurements of the coupling constants is adequate for the $g-2$ experiments at the one part in 10^9 level. On the other hand, unless the accuracy of the coupling constants can be pushed much higher, raising the $g-2$ experiment to even higher precision appears to be very difficult.

ACKNOWLEDGMENTS

We would like to thank R. S. Van Dyck, Jr., F. L. Moore, D. L. Farnham, P. B. Schwinberg, and H. G. Dehmelt for providing us with their data on the cyclotron frequency shifts in a hyperbolic trap. The work was supported, in part, by the U.S. Department of Energy under Contract No. DE-AC06-81ER-40048.

---

[1]The experiments are described by R. S. Van Dyck, Jr., P. B. Schwinberg, and H. G. Dehmelt, Phys. Rev. D **34**, 722 (1986); in *Atomic Physics 9*, edited by R. S. Van Dyck, Jr. and E. N. Fortson (World Scientific, Singapore, 1984), p. 53.

[2]A review of the theory of the experiments is provided by L. S. Brown and G. Gabrielse, Rev. Mod. Phys. **58**, 233 (1986).

[3]R. S. Van Dyck, Jr., P. B. Schwinberg, and H. G. Dehmelt, Phys. Rev. Lett. **59**, 26 (1987).

[4]G. Gabrielse and H. Dehmelt, Phys. Rev. Lett. **55**, 67 (1985).

[5]D. G. Boulware, L. S. Brown, and T. Lee, Phys. Rev. D **32**, 729 (1985), start with the fully relativistic theory of quantum electrodynamics and prove that the only experimentally measurable effect of cavity walls on the $g-2$ experiment is a shift of the cyclotron frequency, which may be computed classically.

[6]The shift for a cylindrical cavity that crudely models an actual Penning trap is worked out in detail by L. S. Brown, G. Gabrielse, K. Helmerson, and J. Tan, Phys. Rev. Lett. **55**, 44 (1985); Phys. Rev. A **32**, 3204 (1985).

[7]The shape of the cavity is very important, as shown by the calculation for a sphere given by L. S. Brown, K. Helmerson, and J. Tan, Phys. Rev. A **34**, 2638 (1986).

[8]This definition differs slightly from that used in Ref. 6.

[9]The electrostatics of such a trap were worked out by G. Gabrielse and F. C. MacKintosh, Int. J. Mass Spectrom. Ion Phys. **57**, 1 (1984). The cylindrical trap with $R/L=1.186$ is currently being tested experimentally by G. Gabrielse and J. Tan (unpublished).

[10]The LANL-DESY program URMEL is described by T. Weiland, DESY Report No. 82-24, 1982 (unpublished).

[11]R. S. Van Dyck, Jr., F. L. Moore, D. L. Farnham, P. B. Schwinberg, and H. G. Dehmelt, Phys. Rev. A (to be published).